Chapitre 5 :

Conclusions de la Partie I

5 Conclusions de la Partie I

La croissance des couches minces de manganites a été réalisée avec succès après le développement d'une nouvelle chambre d'ablation laser. Nous avons décrit dans l'annexe A la procédure suivie pour la conception, le développent et la mise au point de cette enceinte conçue pour le dépôt d'oxydes.

L'originalité de ce travail est:

a) L'étude du transport dépendant du spin à travers des interfaces de grains de manganites ferromagnétiques et métalliques. Pour cette étude, nous avons créé des systèmes modèle avec des joints de grains réalisés par des méthodes nouvelles dans les couches de manganites.

b) L'étude structurale et magnétique complète sur des couches bien caractérisées permettant de déterminer les effets de la contrainte biaxiale induit par la croissance épitaxiale.

Dans le chapitre 3, nous avons montré que la croissance de couches sur des substrats rayés ou avec de paramètres cristallins non accordés ainsi que la déformation de couches par la méthode de la scie atomique, sont des systèmes modèles pour étudier l'effet des joints de grain dans le transport dépendant du spin.

Une étude structurale, de transport et magnétique de films granulaires texturés ou non de $La_{2/3}Ca_{1/3}MnO_3$(LCMO) sur des substrats de MgO avec des paramètres cristallins non accordés a été réalisée et a permis de déterminer les meilleurs paramètres de dépôt ainsi que l'existence d'une plage de température de 100 degrés pour le dépôt de couches de manganite de haute qualité. Au-delà de cette plage, les couches sont polycristallines.

Les études sur ces films ont montré que le transport électrique dans les systèmes granulaires est fortement inhomogène et de type percolatif, même si les couches présentent une résistivité macroscopique de type monocristallin.

Le transport à travers les interfaces a été identifié comme du tunneling inélastique dépendant du spin entre grains voisins et la barrière électrique existante entre certains grains voisins a été associé à la surface des grains. Nos mesures de potentiomètrie ainsi que les mesures de transport électrique sur des joints de grain créés par la méthode de la scie atomique ont montrées que les joints de grains isolants sont des zones de désordre cristallographique dans lesquelles l'interaction de Double Echange est fortement affaiblie. L'hypothèse de l'existence d'une autre phase chimique entre les grains a été rejetée. De plus, les mesures de la magnétorésistance et de l'effet Kerr polaire à haut champ

magnétique font penser que la surface des grains possède un ordre ferromagnétique non saturé, ce qui confirmerait l'hypothèse d'une réduction de l'interaction de Double Echange aux surfaces des grains.

La magnétorésistance à bas champ (LFMR) observé dans les systèmes granulaires a été trouvé comme étant dépendante du désalignement cristallographique des grains et elle varie dans des champs magnétiques de l'ordre du champ coercitif et est indépendante de la taille des grains.

La localisation à basse température a été attribuée à un comportement de type "hopping" ou tunnel inélastique dépendant du spin via des états localisés dans la barrière. Les mesures de résistivité à 30mK ont indiquées l'existence d'effets Magneto-Coulomb pour certains chemins électriques dans les films polycristallins.

Dans le chapitre 4, une étude structurale de l'effet de la contrainte épitaxiale sur les propriétés structurales, électriques et magnétiques du LCMO est effectuée. En raison de la grande interaction électron-phonon, les propriétés magnétiques et de transport des manganites sont très sensibles aux déformations du réseau. Une épaisseur critique pour la relaxation de la contrainte dans le système LCMO sur STO a été trouvée d’environ 60nm. La déformation tétragonale induite par la contrainte epitaxiale dans les couches de LCMO provoque une augmentation de la résistivité résiduelle des couches et une réduction de la température de la transition métal/isolant. Les mesures magnétiques sur les couches contraintes de LCMO sur des substrats de STO montrent l'apparition d'une anisotropie magnétique uniaxiale.

5 Conclusions to Part I

The growth of thin films of manganites has been successfully achieved after our development of a new ablation chamber for oxides deposition. We have described in Appendix A: the procedure followed in its design, development and built up.

The originality of the present work lies on:

1. The study of the spin transport through the grain interfaces of ferromagnetic and metallic manganites. To perform this study we have developed model systems with grain boundaries obtained by new methods in manganite thin films.
2. The extensive magnetic and structural study on well characterised films which allowed to determine the effects epitaxial strain on the properties of manganites.

In chapter 3, we have shown that the thin film growth on scratched substrates, or on mismatched substrates as well as the plastic deformation of the films by the atomic saw method, have allowed to create different model systems where the effect of the grain boundaries on the spin dependent transport through the grain boundaries in manganites has been studied.

A study of the structural, transport, and magnetic properties of granular textured or non textured films of $La_{2/3}Ca_{1/3}MnO_3$ on highly mismatched MgO substrate has been performed and determined the best deposition conditions as well as the existence of a range of deposition temperatures of 100 degrees for obtaining high quality manganite films. Higher and lower deposition températures give rise to polycrystalline films.

The studies on these films have shown that the electrical transport in granular systems is highly inhomogeneous and percolatif even if the films show a single-crystal type macroscopic resistivity.

Transport through the interfaces has been identified to be by spin dependent inelastic tunneling between neighbouring grains and the electrical barrier existent between certain grains has been found to correspond to the grain surface. The potentiometric measurements as well as the measurements on the grain boundaries created by the atomic saw method have shown that the insulating grain boundaries are zones of crystallographic disorder where the double exchange interaction is weakened. . The hypothesis of the existence of a new chemical phase between the grains has been rejected. In addition, magnetoresistance and Kerr effect measurements under high fields agree with the idea of a weakened ferromagnetic state at the grain surface which agrees with the hypothesis of a reduction of the strength of the double exchange interaction at the grain surface.

The LFMR associated to granular systems was found to be dependent on the crystallographic misalignment of the grains, to vary on fields of the coercive field range and to be independent on the grain size.

Low temperature localisation has been attributed to hopping or inelastic spin tunneling through localised states in the barrier. Resistivity measurements at 30mK revealed the existence of Magneto-Coulomb effects in certain electrical paths of polycrystalline films.

In chapter 4, a structural study on the effect epitaxial strain on the structural, electrical and magnetic properties of LCMO is carried out. Due to the large electron-phonon interaction, the magnetic and transport properties of manganites are very sensitive to lattice distortions. A critical thickness for the relaxation of the stress has been found to be about 60nm in the system LCMO on STO. The tetragonal distortion induced by the substrate in LCMO films has shown to increase the residual resistivity of the films and to reduce the FM/Metallic to PM/Insulating transition temperature. Magnetic measurements on strained LCMO films on STO substrates in the out of plane direction, revealed the apparition of a uniaxial magnetic anisotropy.

Partie II

Introduction à la Partie II

Un des sujets les plus intéressants dans les manganites, outre la magnétorésistance colossale, est l'étude des différentes configurations de l'ordre de charge et des phénomènes de ségrégation électronique de phase. Dans les prochains chapitres, les mécanismes à l'origine de la ségrégation de phase seront discutés et analysés à partir de mesures de diffraction de neutrons et de Rayons X et de la relaxation de muons en champ nul, ainsi qu'avec des techniques de caractérisation macroscopique comme l'aimantation et la résistivité. Les différents degrés de liberté: charges, spin, réseaux et orbitaux déterminent les propriétés étonnantes de ces composées.

Dans le chapitre 6, la transition métal isolant associée à la transition structurale de $Pr_{1/2}Sr_{1/2}MnO_3$ à T_N est expliquée à l'aide d'une ***redistribution des charges*** dans laquelle les électrons ont une tendance à migrer vers les plans FM qui sont AFM couplés. Cette migration des charges s'interprète à partir de la stabilisation d'un ordre orbital de type x^2-y^2 et du début de l'ordre magnétique.

Dans le chapitre 7, la ségrégation de phase à l'origine de l'état hétérogène à basse température de $Pr_{2/3}Ca_{1/3}MnO_3$ a été étudiée. La description de la ségrégation de phase ainsi que sa distribution spatiale est basée sur des mesures de diffraction de neutrons et de relaxation de muons. Une étude comparative avec le composé $Pr_{1/2}Ca_{1/2}MnO_3$ à ordre de charge a été réalisée.

Dans le chapitre 8, nous avons réalisé une étude détaillée et systématique des composé de la famille $Bi_{1-x}Ca_xMnO_3$ fortement dopée en trous. Une étude comparative avec les composés à base de lanthane a été réalisée afin de comprendre le rôle du "lone pair" du Bi^{+3}. A partir de techniques de diffraction à haute résolution, nous avons déterminé de façon non équivoque la direction de propagation de la modulation structurale dans les composés qui présentent un l'ordre orbital. Des phénomènes de ***séparation de phase macroscopique*** ont été trouvés et caractérisés dans les composés fortement dopés en trous. Leur comportement magnétorésistif a été interprété sur la base d'un modèle de percolation.

Introduction to Part II

One of the most interesting topics in manganese perovskites apart from the colossal magnetoresistance, is the question of the charge ordered configurations and phase segregation phenomena. In the following chapters different mechanism leading to phase segregation will be discussed and analysed on the basis of detailed neutron and synchrotron X-Rays powder diffraction, muon spin relaxation and macroscopic characterisation techniques as magnetisation and resistivity. The interplay between charge, spin, lattice, and orbital degrees of freedom determines the unusual properties of these compounds.

In chapter 6, the metal-insulator transition associated and orbital ordering in $Pr_{1/2}Sr_{1/2}MnO_3$ taking place at T_N is explained using a thermally induced ***charge redistribution*** in which the electrons tend migrate towards the FM planes that are AFM coupled. This charge migration is interpreted as being originated by the stabilisation of an x^2-y^2 orbital ordering and the onset of the magnetic order.

In chapter 7, the ***electronic phase segregation*** at the origin of the inhomogeneous low temperature state in $Pr_{2/3}Ca_{1/3}MnO_3$ is studied. The description of the phase segregation and spatial distribution of the phases is undertaken based on NPD and μSR data. A comparative study with the CO compound $Pr_{1/2}Ca_{1/2}MnO_3$ has been performed.

In chapter 8, we have developed a detailed and systematic study on the hole rich region of the $Bi_{1-x}Ca_xMnO_3$ family of compounds. A comparative study with the lanthanum based compounds is done to understand the role of the Bi^{+3} lone pair. On the basis of high resolution diffraction techniques we have unambiguously determined the propagation direction of the structural modulations in the compounds exhibiting orbital ordering phenomena. and have analysed the progressive destabilisation of the orbital order. ***Macroscopic phase separation*** has been found and characterised in highly hole doped compounds and their magnetoresistive behaviour has been interpreted based on percolative models.

Chapter 6:

Ordre orbital et transition métal-isolant dans $Pr_{1/2}Sr_{1/2}MnO_3$

6 Ordre orbital et transition métal-isolant dans $Pr_{1/2}Sr_{1/2}MnO_3$

La motivation de ce travail a été d'avoir une meilleure compréhension de l'état fondamental des composés avec un dopage x=1/2, légèrement distordus ($RE_{1/2}Sr_{1/2}MnO_3$). Moins de distorsion dans cette famille donne lieu a des états fondamentaux différents causées par la destabilisation de l'ordre de charge caractéristique pour ces dopages.

Dans ce chapitre, une explication de la transition FM/métallique à AFM/isolant du composé $Pr_{1/2}Sr_{1/2}MnO_3$ est décrite en détail et est basée sur des mesures de diffraction de neutrons de haute résolution.

Nous montrerons que les distorsions cristallographiques associées à transition structurale FM/M - AFM/I peuvent être interprétées comme causées par la migration électronique des charges due à la stabilisation d'un ordre orbital de type $d_{x^2-y^2}$ dans les plans ferromagnétiques.

6 Orbital ordering and metal-insulator transition in $Pr_{1/2}Sr_{1/2}MnO_3$

The motivation of the present work has been to get insight into the ground state of the compounds with x=1/2 doping slightly distorted ($RE_{1/2}Sr_{1/2}MnO_3$). Less distorted compounds in this family gives rise to different fundamental states due to the destabilisation of the charge and orbital ordering characteristic of these doping levels.

In this chapter, an explanation of the FM/metallic to AFM/insulating transition of $Pr_{1/2}Sr_{1/2}MnO_3$ is described in detail based on high-resolution neutron powder diffraction.

It will be shown that the crystallographic distortions related to the structural transition associated to the FM/M - AFM/I transition, can be interpreted to be originated by the migration of the charges towards the FM planes and the stabilisation of a $d_{x^2-y^2}$ orbital order.

6.1 Introduction

The structural and magnetic properties of the series of compounds $RE_{1/2}Sr_{1/2}MnO_3$ evidence the competing interactions existing in manganite compounds when the bandwidth gets narrower [145]. The ground state of these materials is very sensitive to the rare earth (RE) size as well as to the substitution of Sr by Ca because the bandwidth is intimately related to the tilting of the oxygen octahedra.

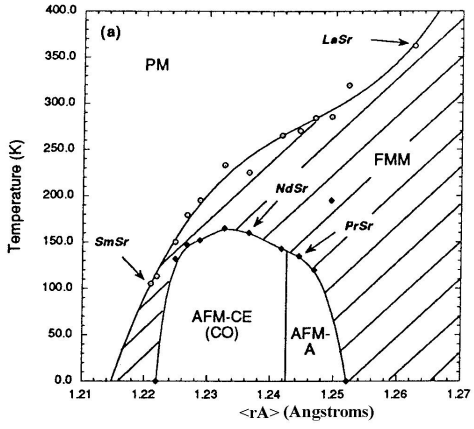

Fig. 6-1 Phase diagram for $RE_{0.5}Sr_{0.5}MnO3$ as a function of $<r_A>$ extracted from [145]

In Fig. 6-1 is shown the phase diagram of the $RE_{1/2}Sr_{1/2}MnO_3$ series of compounds as a function of the A site averaged radius ($<r_A>=(r_A + r_{Ln})/2$). Its inspection reveals the competition between FM and AFM-CE charge ordered states and AFM-A states. When the rare earths (RE) are big, the FM/metallic state is stabilised at low temperatures. Upon doping with smaller RE the FM state is destabilised and an A-type AFM state becomes the ground state. The A–type AFM order consist in FM planes coupled AFM (Fig. 6-2). This type of magnetic order could coexist with a charge ordered or charge disordered state. In the former case, the FM planes would be insulating while in the second case they would be metallic.

For smaller RE radius, the CE type magnetic structure is stabilised and implies the ordering of the charges and d_z^2 orbitals.

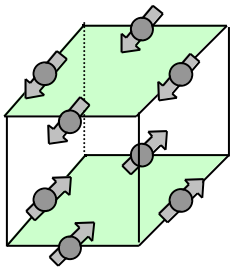

Fig. 6-2 *Schematic image of the A-type AFM ordering with FM planes coupled AFM.*

So, while $La_{1/2}Sr_{1/2}MnO_3$ is a ferromagnet at low temperatures ($T_C \approx 340K$), $Pr_{1/2}Sr_{1/2}MnO_3$ and $Nd_{1/2}Sr_{1/2}MnO_3$ display AFM structures at low temperature ($r_A(La) > r_A(Pr) > r_A(Nd)$). Nevertheless, the nature of their magnetic structures is very different:

a) $Nd_{1/2}Sr_{1/2}MnO_3$ displays charge ordering (CO) at low temperature [146] and an AFM CE type structure with two different magnetic sublattices (Mn^{+3} and Mn^{+4} with different propagation vectors).

b) $Pr_{1/2}Sr_{1/2}MnO_3$ compound is situated in the bordering region between AFM-CE and FM states. Some authors claimed to have observed AFM-CE and CO in this compound [147] but detailed studies based on neutron diffraction measurements revealed that such structure is not found.

Our neutron diffraction measurements do not display any superstructure peaks corresponding to a doubled cell that would be observed in an AFM-CE superstructure. An A-type AF structure was found at low temperatures in this compound and the metal to insulator transition is accompanied by a structural transition. This A-type AFM structure has been also predicted to be the ground state of $Pr_{1/2}Sr_{1/2}MnO_3$ from Hartree-Fock calculations [148]. The analysis we have performed of the structural transition permits to understand the role a particular orbital ordering on the stabilisation of the magnetic ordering and rules out the existence of a CO state in this compound.

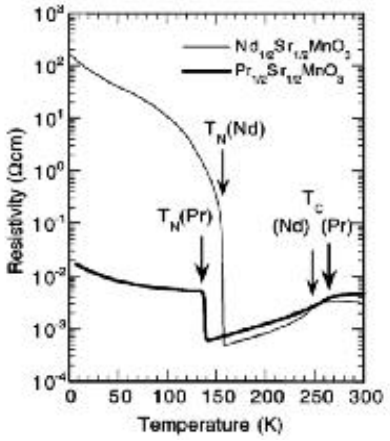

Fig. 6-3 *Resistivity measurements extracted from [149] displaying the differences in the resistivity in the AFM state for single crystals of A-type AFM $Pr_{1/2}Sr_{1/2}MnO_3$ and the AF-CO $Nd_{1/2}Sr_{1/2}MnO_3$.*

The ordering of the charges (CO) exists when the long range Coulomb interaction of charge carriers among the carriers overcomes the kinetic energy of the carriers. The A-type AFM charge ordered state is favoured when the x^2-y^2 e_g orbital is occupied at the Mn^{+3} sites. This ordering would imply a cooperative breathing-type lattice distortion with the Mn^{+3} and Mn^{+4} associated octahedra alternatively expanded and contracted in the FM planes. From calculations is extracted that this kind of orbital, charge and magnetic ordering seem to be unstable when the tilting of the octahedra is too small [149].

In the absence of charge ordering, the Double Exchange (DE) interaction could be possible in the FM planes and thus they would be metallic. However, neighbouring planes are AFM in the A-type AFM ordering. The coupling between FM planes is thus governed by the superexchange interaction between t_{2g} orbitals and no conduction is possible. In the case, where metallic conduction is possible within the FM planes and not in the direction perpendicular to them the material would behave as a metallic antiferromagnet, and thus its transport properties would be highly anisotropic.

In Fig. 6-3 are shown the resistivity measurements at zero applied field for the $Nd_{1/2}Sr_{1/2}MnO_3$ AFM-CO and the $Pr_{1/2}Sr_{1/2}MnO_3$ A-type AFM single crystals as extracted from [149]. It can be observed that the residual resistivity of $Pr_{1/2}Sr_{1/2}MnO_3$ sample is nearly four orders of magnitude lower than the CO sample. This is an indication that carriers are more mobile in the case of $Pr_{1/2}Sr_{1/2}MnO_3$. Moreover, two transitions are detected in resistivity measurements. The first one at T_C=267K when a PM/I to FM/M transition takes place and a second at T_N=135K consisting in a FM/M to AFM/I transition.

6.2 Structural and magnetic transition: A Neutron diffraction study

In order to understand the unexpected FM/M to AFM/I transition in $Pr_{1/2}Sr_{12}MnO_3$ we have performed a series of neutron diffraction measurements at the Institute Laue-Langevin in Grenoble. Neutron diffraction data were collected with the high intensity D1B diffractometer (λ=2.52Å) and the high resolution D2B diffractometer (λ=1.5936Å) in its high flux between 1.5 to 300K.

$Pr_{1/2}Sr_{1/2}MnO_3$ powders were prepared as sintered ceramic by standard solid state reaction in air at ICMAB. The concentration of Mn^{+4} was found to be 0.51(1) from chemical analysis.

It is found from NPD analysis that at the FM to AFM magnetic transition, the sample exhibits a structural transition. In Fig. 6-4 is displayed the thermal evolution of a selected

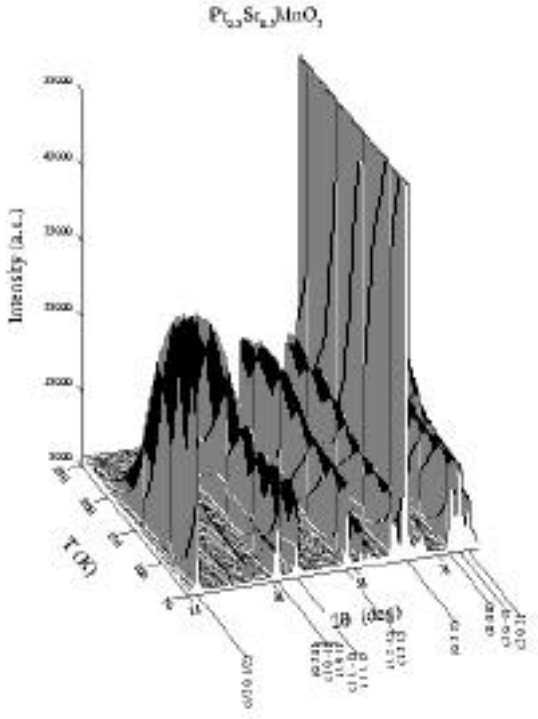

Fig. 6-4 *Detail of the thermal evolution of the neutron diffraction pattern for $Pr_{1/2}Sr_{1/2}MnO_3$*

range of the NPD pattern. On the one hand, it can be observed that certain nuclear peaks exhibit an increase and lately a decrease of their intensity. This corresponds to the apparition of FM in the temperature range between 140K to 270K. The decrease of the FM intensity is accompanied by the apparition of new peaks at low angles, which can be associated to the onset of long range AFM order. Another interesting feature is that the onset of the apparition of the AFM is accompanied with the apparition of new Bragg peaks, which corresponds to the crystal symmetry change.

The fact that the structural transition appears at the AFM ordering temperature, T_N, is not common in x=1/2 samples exhibiting CO. In $Ln_{1/2}Ca_{1/2}MnO_3$ samples exhibiting AFM CE and CO ground state at low temperatures the structural transition appears at the CO temperature and no structural change occurs at T_N.

At RT, $Pr_{1/2}Sr_{1/2}MnO_3$ is tetragonal with a space group I4/mcm. This tetragonal structure is obtained from the primitive cubic perovskite by the rotation of the MnO_6 octahedra around the c axis ($a^0a^0c^-$ following Glazer's terminology[150]). The sense of the rotation changes when successive octahedra are considered along the c axis. In Fig. 6-5 is shown the refinement obtained at RT from the D1B NPD data used also to follow the thermal evolution of the cell parameters. The results of the refinements are shown in Tab. 6-III.

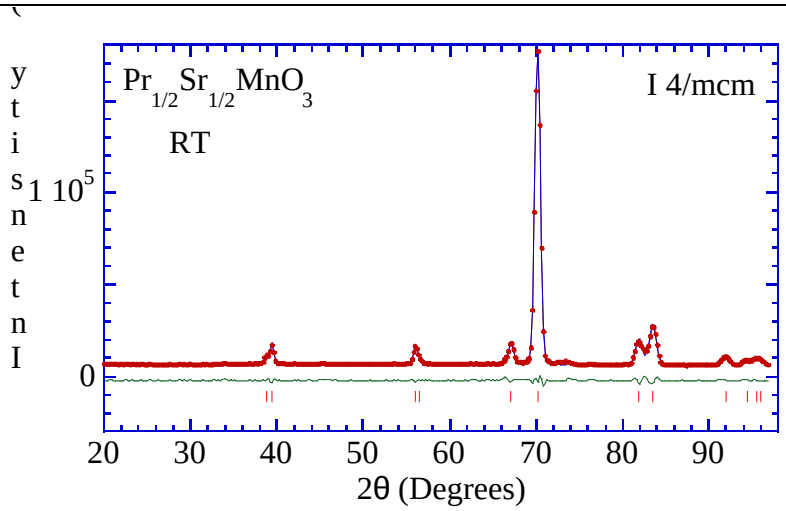

Fig. 6-5 *Observed (circles) and calculated (line) neutron-diffraction pattern of $Pr_{1/2}Sr_{1/2}MnO_3$ at RT from D1B NPD data.*

The thermal evolution of the cell parameters is shown in Fig. 6-6. Upon cooling down the sample, the intensity of the (110) Bragg peak increases around 268K (T_C) illustrating the onset of three dimensional ferromagnetism coinciding with the metallic state. No structural transition is observed at the PM to FM transition.